Int J Adv Manuf Technol (2013) 69:1185–1201
DOI 10.1007/s00170-013-5053-3

ORIGINAL ARTICLE

Deformation mechanics in single-point and accumulative double-sided incremental forming

Jacob Smith · Rajiv Malhotra · W. K. Liu · Jian Cao

Received: 13 November 2012 / Accepted: 1 May 2013 / Published online: 14 June 2013

Abstract Single-point incremental forming (SPIF) uses one small hemispherically ended tool moving along a predefined toolpath to locally deform a completely peripherally clamped sheet of metal such that the sum total of the local deformations yields the final desired shape of the sheet. While SPIF is characterized by greater formability than conventional forming processes, it suffers from significant geometric inaccuracy. Accumulative double-sided incremental forming (ADSIF) is a substantial improvement over SPIF in which one hemispherically ended tool is used on each side of the sheet metal. The supporting tool moves synchronously with the forming tool, therefore acting as a local but mobile die. ADSIF results in considerably enhanced geometric accuracy and increased formability of the formed part as compared to SPIF. In light of the aforementioned advantages of ADSIF as compared with SPIF, an investigation of the mechanics associated with the ADSIF process, which has yet to be presented in the literature, is warranted. The present study sheds light on the differences in deformation mechanisms between SPIF and ADSIF. Finite element analyses are performed to simulate deformation in the two processes, and a detailed analysis of the deformation history is presented. It is shown that the presence of the supporting tool in ADSIF elicits substantial differences in the plastic strain, hydrostatic pressure, and shear strains as compared to SPIF. The implications of these trends on the prevalent modes of deformation in ADSIF along with possible explanations for increased formability observed in the process are discussed.

J. Smith · R. Malhotra · W. K. Liu · J. Cao (✉)
Department of Mechanical Engineering, Northwestern University, 2145 Sheridan Rd., Evanston, IL 60208-3111, USA
e-mail: jcao@northwestern.edu

Keywords Accumulative double-sided incremental forming · Single-point incremental forming · Deformation mechanics · Finite element analysis

1 Introduction

Incremental forming is a low-volume production, or rapid-prototyping, process which has received much attention in the automotive, biotechnology, aerospace, and defense manufacturing industries due to its increased formability, reduced forming forces, and the removal of the need for product-specific dies. Single-point incremental forming (SPIF) is the simplest form of incremental forming. In SPIF, a sheet of material is clamped peripherally and deformed locally using a single tool moving along a predefined toolpath. The accumulation of these local deformations amasses to impart a final desired shape to the sheet. SPIF is characterized by increased formability as compared to conventional processes but is plagued by a lack of geometrical accuracy of the final product [5]. Double-sided incremental forming (DSIF) was an improvement on the SPIF process in which a second tool was used on the opposite side of the sheet, acting as a local support for the forming tool, which improved the geometric accuracy as compared to SPIF. However, loss of contact between the tools and the sheet was observed as deformation increased which resulted in inadequate geometrical accuracy of the formed component [5]. One solution proposed to alleviate this issue involved using combined force and displacement control such that the supporting tool maintains contact with the sheet throughout the forming process [8]. While this approach was determined to successfully maintain contact between the supporting tool and the sheet during DSIF, the control mechanism requires the determination of parameters which depend on the shape

of the part being formed. The parameters used in this control strategy have to be obtained via iterative experimentation which reduces the highly advantageous flexibility of the incremental forming process.

Accumulative double-sided incremental forming (ADSIF) is a recently developed [6] enhancement of DSIF which can significantly improve geometric accuracy and increase formability without using any shape-specific tooling or dies and with no loss of contact between the sheet and the tools during forming. In a conventional out-to-in (SPIF or DSIF) toolpath (Fig. 1a), the tool moves in the negative Z-direction by an incremental depth ΔZ, deforms the sheet along a shape-specific XY-profile at that depth, then moves down by another ΔZ, and repeats the process until the tool reaches the final depth of the component to be formed. In ADSIF (Fig. 1b), the toolpath is designed such that the tools form an annulus of the material to the specified incremental depth ΔZ and then travel outward in the plane of the sheet forming another annulus of undeformed material until a depth ΔZ, thus causing the previously formed annulus to move in the negative Z-direction to a new depth that is twice the previous depth. This process repeats until the entire component is formed. Figure 2 shows a schematic of the tool positioning strategy in ADSIF. The top tool (forming tool) is positioned based on its diameter, the incremental depth, and the local normal of the desired shape at the contact point as in conventional out-to-in toolpaths. The positioning of the second tool is such that the line joining the centers of the top and bottom tools passes through the desired contact point of the top tool (Fig. 2).

This strategy can also be generalized to form complex free-form components with features on either side of the sheet (Fig. 3a). It has been shown experimentally that ADSIF results in improved geometric accuracy (Fig. 3b) and increased formability (Fig. 3c) as compared to SPIF and DSIF. It is important to note here that the components shown in Fig. 3c were formed with the same wall angle in the ADSIF, SPIF, and DSIF cases. The reason that a lower depth of the formed components is shown in the case of SPIF and DSIF out-to-in toolpaths is that the forming process was stopped once the sheet metal had fractured. On the other hand, the sheet did not fail during the ADSIF process.

A significant amount of research related to incremental forming processes has focused on pinpointing the fundamental mechanics of the plastic deformation evolution and fracture in order to fully utilize the increased formability observed in the process. Jackson and Allwood [4] conducted an experimental investigation of incremental sheet forming (ISF) for both the two-point incremental forming (TPIF) and SPIF processes. The TPIF process is similar to the SPIF process but utilizes a prefabricated stationary die on the opposite side of the sheet from the tool. The authors concluded that the primary deformation mechanisms in both SPIF and TPIF are bending, stretching, and shear perpendicular and parallel to the tool motion. Furthermore, they showed that the shear along and perpendicular to the tool motion is much higher in ISF than in conventional forming processes. This is different from the previously popular assumption of pure shear through the thickness of the sheet with plane strain along the component wall. It was also proposed that the shear perpendicular to the tool motion was

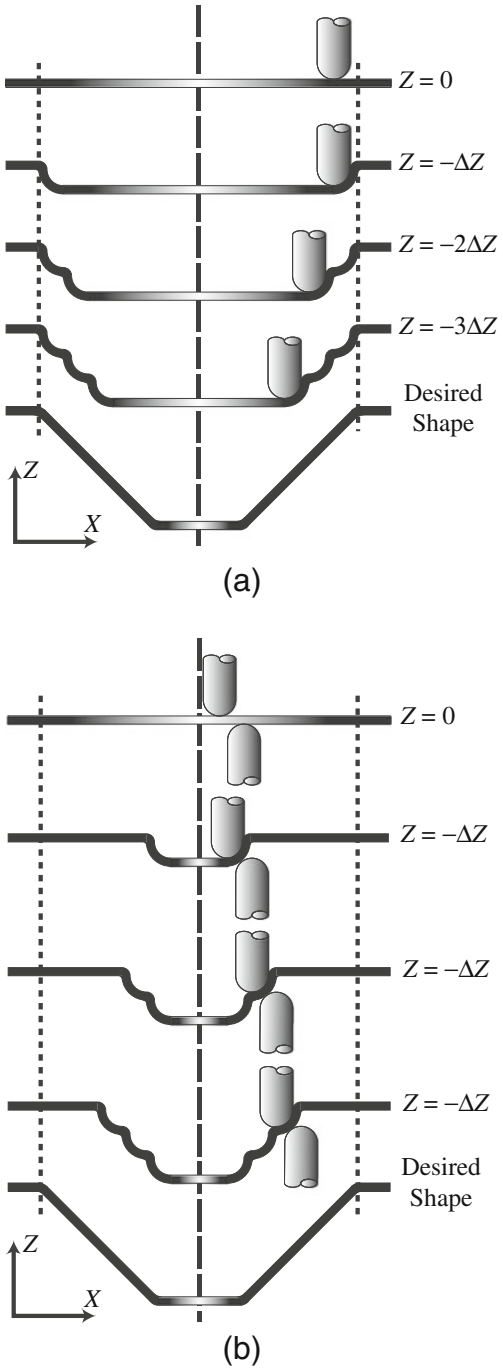

Fig. 1 Schematic of (**a**) conventional SPIF out-to-in toolpath and (**b**) ADSIF toolpath

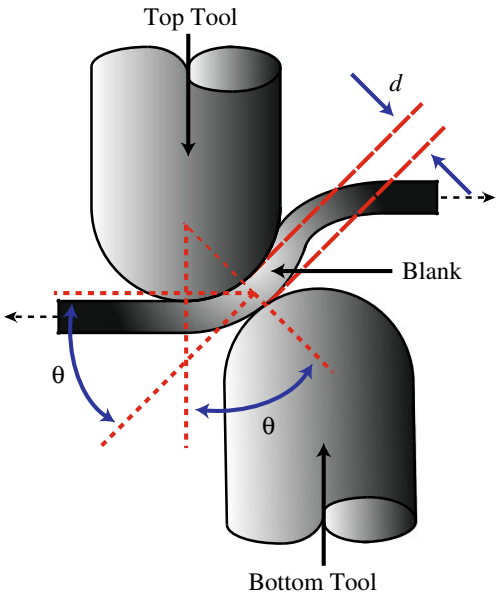

Fig. 2 Tool positioning strategy in ADSIF

caused by (1) material build-up as the tool progresses along the profile of the feature and (2) tool rotation. Jackson and Allwood [4] also commented on the increased forming limit seen in ISF processes and proposed that increasing shear during plastic deformation might be the reason for increased formability.

The aforementioned work was also supported by Allwood and Shouler [1] who devised a method using a generalized forming limit diagram (GFLD) which incorporates the possibility of all six components of the symmetric stress tensor to be nonzero. This GFLD therefore takes into account the characteristic deformation mechanics of normal stresses and through-the-thickness shear in incremental forming, unlike traditional FLDs in which the underlying assumption is that the deformation is plane stress. Emmens et al. [2] attempted to explain the enhanced formability seen in incremental forming processes by reviewing six modes of deformation, i.e., (1) contact stress, (2) bending under tension, (3) shear, (4) cyclic straining, (5) geometrical inability of a shear band to grow, and (6) hydrostatic pressure. However, they did not pinpoint the contributions of the deformation mechanisms towards increasing formability in ISF processes beyond that of traditional processes.

Silva et al. [9] used a membrane analysis incorporating hydrostatic pressure-dependent damage and ductile material failure. Based on experimental observations for the SPIF process, they also proposed that fracture in SPIF is not preceded by localized necking. However, Silva did not directly include through-the-thickness shear effects in the model which are a significant deformation mechanism in incremental forming. Silva et al. [10] later conducted a study to characterize the mechanics of deformation in SPIF by

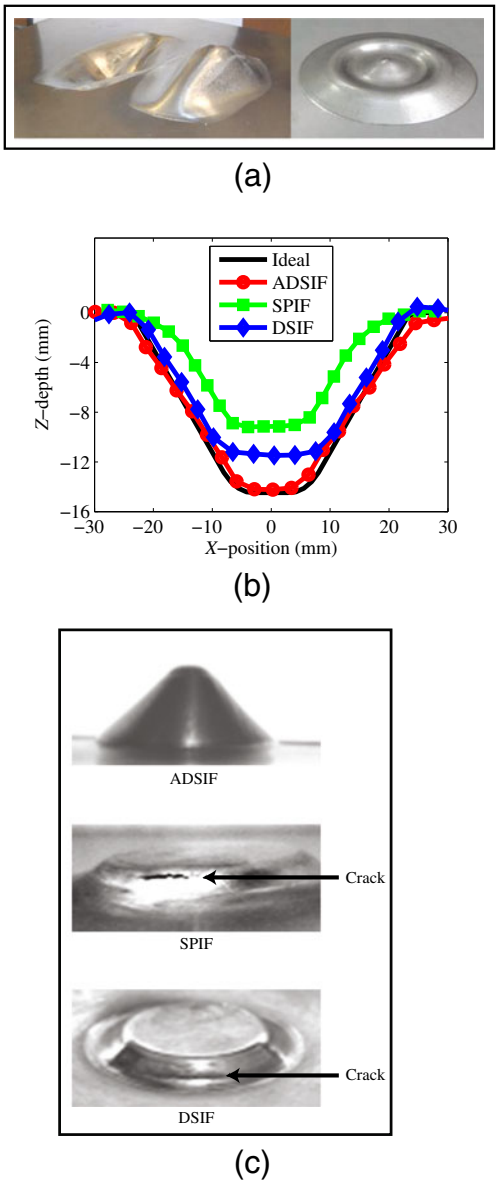

Fig. 3 **a** Complex geometries formed using ADSIF on both sides of the sheet. **b** Improved geometric accuracy of ADSIF as compared with SPIF and DSIF, and **c** increased formability in ADSIF as compared with SPIF and DSIF for a 50 degree cone

utilizing a finite element method framework. In this work, Silva proposed that the governing mode of deformation was, in fact, stretching and that fracture occurs without observation of necking. However, the effect of shear on material localization and necking was still not included.

Malhotra et al. [7] used finite element analysis (FEA) with a damage-plasticity model based on Xue's fracture model [11] to simulate the SPIF process and characterize localization [12] in order to investigate material failure during forming explicitly. They reported that the fracture depth, or formability, and the forming forces compared very well with experimental observations. An in-depth analysis of the

deformation history from the FEA was performed to quantify the individual effects of local bending and shear on sheet metal failure during SPIF. Drawing from observations made during the aforementioned work [7] as well as experimental observations of ADSIF, the same authors proposed that increased compression of the sheet along with increased through-the-thickness shear might be responsible for the increased formability observed in ADSIF as compared to SPIF [6].

Fan et al. conducted sheet metal forming simulations of the deep drawing process and discussed the necessity of proper selection of process speedup parameters for low-speed forming processes in explicit FEA in order to avoid inertial effects. They further examined the effect of increasing the feed rate in the simulation and found that there were large variations in the punch force [3]. In order to conduct the FEA study on the SPIF and ADSIF processes in a reasonable amount of time, the feed rate in the simulations were increased drastically over the experimental feed rate, and erroneous inertial effects were observed. For the present study, the authors have developed a modeling procedure which can greatly improve the capability of process speedup in sheet metal forming processes which are characterized by highly localized deformation, e.g., the SPIF, DSIF, and ADSIF processes.

In light of the previously mentioned advantages of ADSIF over SPIF as well as previous works covering the deformation mechanics in SPIF, the governing mechanisms promoting increased formability in ADSIF as compared with SPIF deserves closer attention. The purposes of the present work are to (1) develop a FEA modeling procedure for SPIF and ADSIF processes, (2) pinpoint the differences in deformation mechanics of SPIF and ADSIF using the deformation history obtained from the FEA, and (3) discuss the possible reasons for increased formability in ADSIF based on the deformation mechanics. The FEA model developed herein to characterize the differences in the two processes is implemented using a piecewise linear elastic-plastic constitutive model to govern the stress–strain behavior of the sheet material. Simulations were performed for SPIF by forming a 40° cone and for ADSIF by forming a 35° cone with the same process parameters. Appreciable elastic springback has been experimentally observed in the SPIF process leading to the choice of different target wall angles to ensure that the actual formed angle and depth in the two cases is similar. The choice of the target wall angles were selected based on the experimental experience of the authors. Section 2 briefly discusses the experimental setup and machine for performing the SPIF and ADSIF processes in order to provide physical reference for the process modeling technique used in the FEA. A detailed overview of the process parameters, material model, and meshing utilized within the simulations is described in Section 3. Section 4 gives a comparison of the mechanics observed from the deformation history for each process. A discussion on the impact of each type of deformation mechanism is outlined in Section 5, followed by concluding remarks and future work in Section 6.

For the purposes of this study, the focus is only on SPIF and ADSIF because the conventional out-to-in DSIF process (Fig. 1a) is characterized by a loss of contact between the sheet and the supporting tool [5], and intuitively, the ADSIF process will have a hybrid set of mechanics comprising those seen in the SPIF and DSIF processes.

2 Experimental setup

In the SPIF experimental setup, a square-shaped sheet of material is peripherally clamped along all outer edges. A conventional out-to-in toolpath is used in which the deformation begins with features on the neutral plane of the sheet and ends at the locations of the deepest features of the final product geometry. Analogous to the SPIF experimental setup, a sheet of material in the ADSIF process is peripherally clamped in the machine along all outer edges. The ADSIF process requires the use of two tools, one on either side of the sheet (one for forming and the other for acting as a local die). To synchronize the motion of the two tools in ADSIF, the speed of the first tool (forming tool) is set by the user, and the speed of the second tool (supporting tool) is automatically calculated based on the preprogrammed displacements of the forming tool and the relative locations of the forming and supporting tools. The experimental setup used for these experiments was previously developed by the co-authors and is shown in Fig. 4. The maximum in-plane forming area for this setup is 250 mm by 250 mm with strain gauge-based load cells mounted on each tool for measuring forming forces during the forming process.

For the SPIF experiment, a cone with a wall angle of 40° was formed on a 0.5-mm-thick AA2024 sheet using a 5.0-mm diameter tool. The toolpath used was a conventional out-to-in contour toolpath with an incremental depth of 0.025 mm at a feed rate of 5 mm/s. The rotational degree of freedom of the tool was completely constrained during deformation. The lubricant used at the tool–sheet interface incorporates a petroleum jelly base with suspended graphite particles. The lubricant is applied liberally throughout the entire experiment which drastically reduces the impact of friction for the process. For the ADSIF experiment, a cone with a wall angle of 35° was formed using two 5.0-mm diameter tools, one on each side of the sheet. The sheet material, sheet thickness, incremental depth, tool feed rate, and lubricant used in the ADSIF process were the same as those used in the SPIF process.

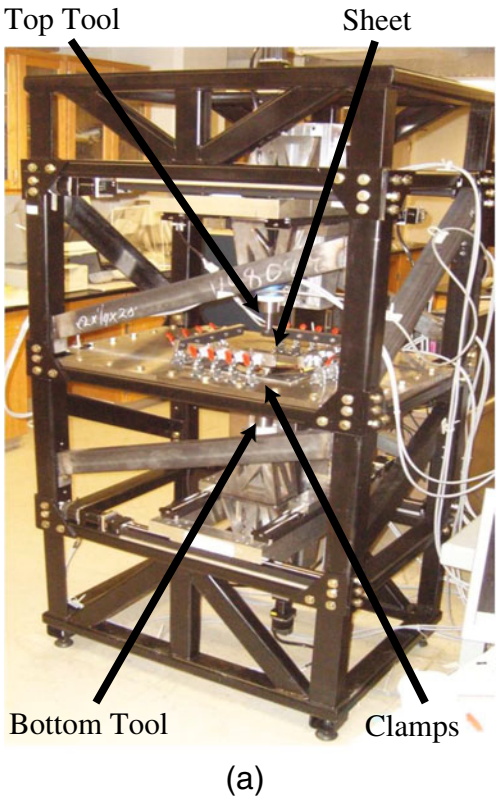

Fig. 4 **a** Prototype incremental forming machine fabricated at Northwestern University. **b** Closeup view of the sheet clamping system

The difference in the designed wall angles for SPIF and ADSIF is to ensure that the final wall angles of the formed feature are similar such that a comparison is justified. SPIF is characterized by a significant amount of elastic bending outside the desired forming area as well as a large amount of springback of the wall after the process is completed. This phenomenon results in the final wall angle of the cone that is formed with SPIF being lower than the designed wall angle (the target wall angle as implemented in the toolpath). Therefore, to make a cone with a final wall angle of about 30° (the actual wall angle) using SPIF, the designed wall angle used to create the toolpath was set to 40°. In ADSIF on the other hand, the geometric accuracy is significantly better, and bending of the sheet outside the forming area is minimal, thus the target wall angle is set to 35° to obtain a 30° final wall angle. Figure 5 shows a schematic of the designed geometry used in the simulations.

The cone geometry shown in Fig. 5 was selected for analysis because of its constant wall angle. By removing the variation in wall angle from the process, we can easily analyze and compare the process mechanics of SPIF and ADSIF without considering their dependence on the formed wall angle. The particular wall angle chosen for this analysis was selected because, experimentally, it has been found that the likelihood of fracture for this component is extremely low. Since the objective of this work is to analyze the deformation mechanisms in two different forming strategies, it is ideal to confine our attention to parts which will not fracture. Finally, the cone geometry is a widely used geometry in the incremental forming research community which

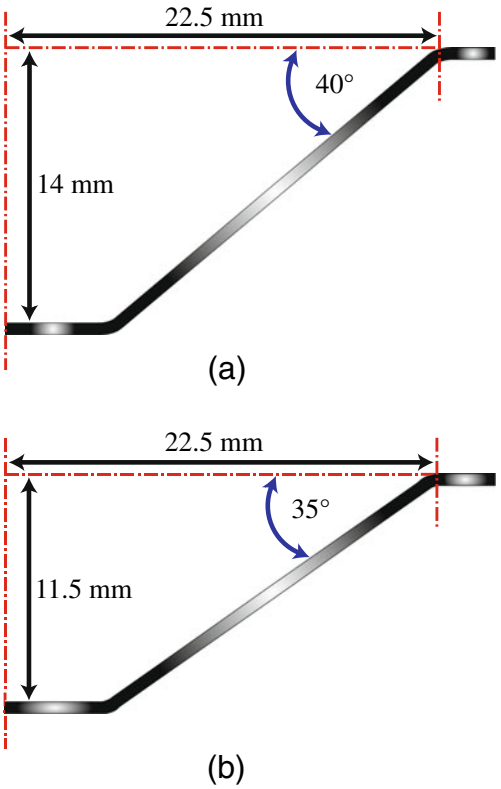

Fig. 5 Profiles of cones used for (**a**) SPIF and (**b**) ADSIF simulations

Table 1 Material properties of AA2024 calibrated from tensile tests

ρ (kg/m^3)	E (GPa)	ν	σ_{y0} (MPa)
2,680	73.1	0.3	282

enables easy comparison of previous and future research with the results presented in this work.

3 Finite element analysis

The finite element analyses described in the present work were performed using LS-DYNA explicit for both the SPIF and ADSIF processes. LS-DYNA was selected as the FEA solver due to its well-established reputation in explicit analysis in terms of better speed of computation as compared with other solvers and also the wide variety of numerical methods which can be implemented for analysis. Explicit FEA was selected for the study because the simulations undergo many small deformation increments during which contact has to be reestablished for a very large mesh size, and thus an implicit solver would be much more time-consuming. Explicit simulations also scale much better than implicit simulations when solving on parallel computing clusters (as was used here).

The components shown in Fig. 5a, b were formed in the simulation of the SPIF process and ADSIF process, respectively, with the aim of examining the deformation mechanics in the two processes. A piecewise linear elastic-plastic material model was used to govern the mechanical response of the AA2024 sheet during the deformation process. The material properties for AA2024 were calibrated from uniaxial tensile testing and can be found in Table 1, and the stress–strain behavior is illustrated in Fig. 6.

A schematic of the FEA model used for the simulations is shown in Fig. 7. To simulate the completely peripherally clamped sheet, as described in the experimental setup,

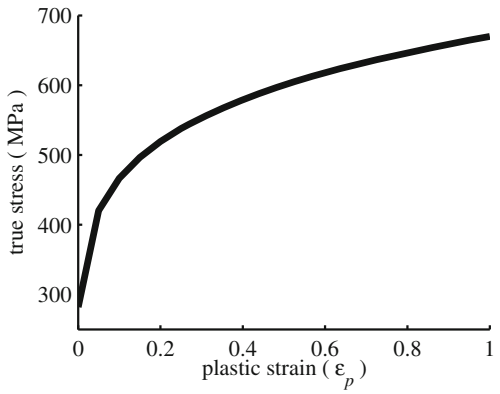

Fig. 6 True stress–strain curve used to model AA2024 material response in FEA during deformation

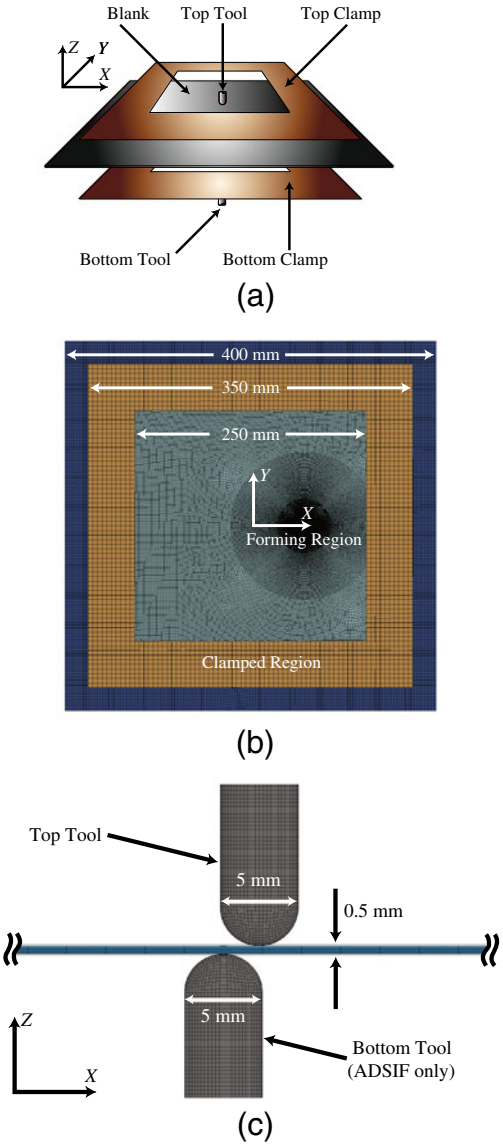

Fig. 7 Schematic of FEA model showing (**a**) an exploded view of the solid model, (**b**) the meshed model (excludes tooling), and (**c**) the two tools used to deform the sheet in the ADSIF process

a fixed encastre boundary condition was applied to the eight corner nodes of the sheet. Therefore, the material was impeded from flowing into the forming area during the process. Additionally, a rigid shell enclosure (Fig. 7a, b) consisting of a top clamp and a bottom binder was added along the outer peripheries of the top and bottom surfaces of the sheet. This shell enclosure prevented movement of the clamped region of the sheet in the Z-direction, i.e., normal to the sheet, and friction between the shell enclosure and the sheet provided a further impediment to flow of material into the forming region. The tools were modeled as rigid bodies (Fig. 7c), and friction between the tool/s and workpiece was neglected. Although friction is present to some

extent, it is assumed for the current study that there is no effect of friction between the tool/s and workpiece due to the liberally applied lubricant discussed previously. The impact of friction on the mechanics of the ADSIF process will be investigated in future work.

The Flanagan–Belytschko stiffness-based hourglass control formulation for explicit analysis was used to reduce any zero-energy deformation modes that might have developed during the deformation of the sheet in the simulations. Because the experimental feed rate of the tool/s in the SPIF and ADSIF processes is a quasi-static 5 mm/s, the simulation time required to model the exact process at the experimental speed would be tremendous. To reduce computational time, mass scaling was used to increase the stable time step, and the tool speed (top tool) was increased to 750 mm/s. The speed of the bottom tool was also increased, of course, but only implicitly based on its relative location to the top tool such that the relative preprogrammed positions of the two tools with respect to each other were maintained at all times. Furthermore, because the material selected for the experiments and simulation has been experimentally observed to be highly non-strain rate-sensitive, increasing the tool speed has little to no effect on the sheet material behavior.

During initial studies of the SPIF process using FEA, the simulation was seen to accrue large dynamic oscillations during deformation which were also present in the ADSIF process simulation but were much less detrimental. This was attributed to the fact that in the ADSIF process, the sheet is constrained between the tools, and as a result, the portion of the sheet outside the desired forming region undergoes minimal undesirable deformation. Therefore, increasing the tool speed in ADSIF simulations does not greatly contribute to dynamic instabilities outside the desired forming area but can cause noticeable erroneous results. In SPIF, the deformation is inherently uncontrolled, a fact that has been reported earlier as well [5]. When the tool speed was increased in the SPIF simulation, the dynamic oscillations caused the sheet to vibrate over a large area inducing high-amplitude spurious wave reflections from the clamped boundary of the blank. This caused the simulation to either cease or produce nonphysical results.

To circumvent this issue, global mass damping was added to the system in the SPIF simulation for all six (translational and rotational) degrees of freedom to reduce the onset of dynamic oscillations. Another measure used to reduce spurious wave reflections along the boundary of the sheet in the SPIF simulation was the application of a nonreflecting boundary condition outside the forming area opening, but inside the clamped region. Figure 8 shows the section of the sheet that was selected to have a nonreflecting boundary condition. The ADSIF simulation was conducted using the same global mass damping and nonreflecting boundary conditions as in the SPIF simulation to maintain as much congruency between the model methods as possible.

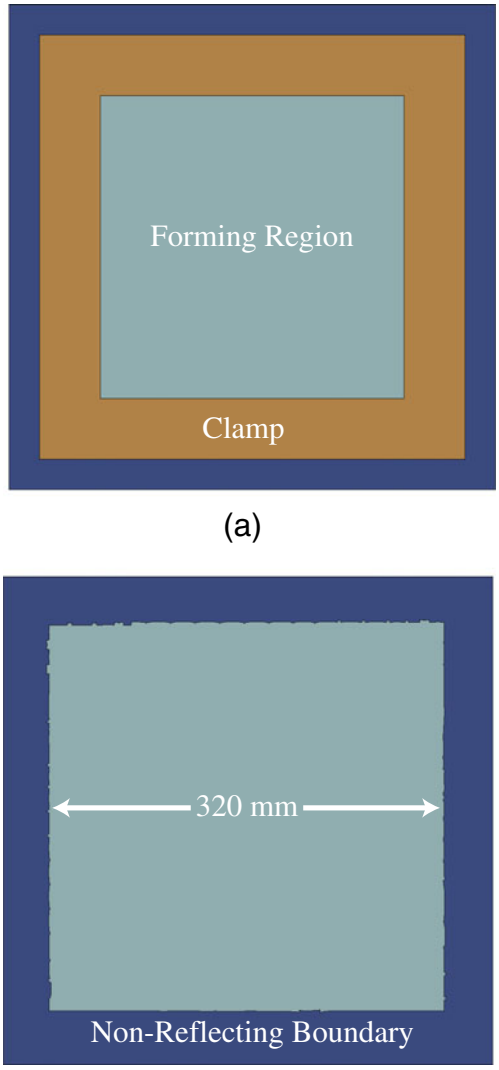

Fig. 8 Schematic of FEA model showing (**a**) the location of the clamps compared to (**b**) the location of the nonreflecting boundary condition applied during the simulations

It is important to note that the forming area of the sheet and the nonreflecting area of the sheet are connected as though they are a single workpiece. However, in order to apply the nonreflecting boundary to the region shown in Fig. 8, the region is required to be assigned as a strictly elastic material. This type of an assumption is only justified by the fact that the area where the condition is applied is completely clamped during experiments and, in a worst case scenario, will incur only elastic deformations. As shown in Fig. 8, the interface between the elastic nonreflecting boundary and the elastic-plastic forming area is enclosed by the top and bottom clamps.

The mesh for the sheet was identical for the SPIF and ADSIF simulations and consisted of 555,768 linear brick elements with reduced integration elements with an average in-plane element size of 0.404 mm by 0.325 mm in the radial direction of the desired forming region. In order to capture the effects in the directions perpendicular (radial) and parallel (tangential) to the motion of the tool, the sheet was radially meshed in the region where contact with the tool is to occur, i.e., where the cone is to be formed. The blank was meshed with eight elements through the thickness in order to model local sheet bending correctly [7]. For both simulations, the top and bottom clamp sections are positioned at 0.06 mm from the top and bottom surfaces of the sheet, respectively. The initial placement of the tools with respect to the sheet is also 0.01 mm from the top and bottom surfaces of the sheet.

Selected details of the SPIF and ADSIF simulations are shown in Table 2. The ADSIF simulation was performed on a parallel computing cluster by utilizing eight nodes with eight processors per node for a total of 56 processors. The SPIF process simulation was performed on the same cluster using six nodes with eight processors per node for a total of 48 processors.

4 Deformation analysis of SPIF and ADSIF

In order to compare the deformation mechanics in SPIF and ADSIF, certain key deformation indicators are plotted as the deformation progresses. These indicators include the plastic strain evolution ϵ_p, hydrostatic pressure p, and the shear strains both parallel ϵ_{ZX} and perpendicular ϵ_{ZY} to the travel direction of the tool. These deformation indicators are plotted at four distinct sections, A to D (Fig. 9a), along the walls of the cones created in the ADSIF and SPIF process simulations. Furthermore, at each of these sections, the indicators are plotted for elements on the inner side (the side in contact with the top forming tool) and outer side (the side in contact with the bottom supporting tool) of the sheet (Fig. 9b). Figure 9 shows the approximate location of each of the four sections in the deformed and undeformed configuration as well as the locations of elements 1 (inner side) and 8 (outer side) along the deformed cone profile for a given section of interest.

Table 2 FEA model details

Case	Tool speed (mm/s)	Time step with mass scaling (s)	Simulation time (days)	Mass damping scale factor
SPIF	750	1.60E-6	24	100
ADSIF	750	1.60E-6	30	100

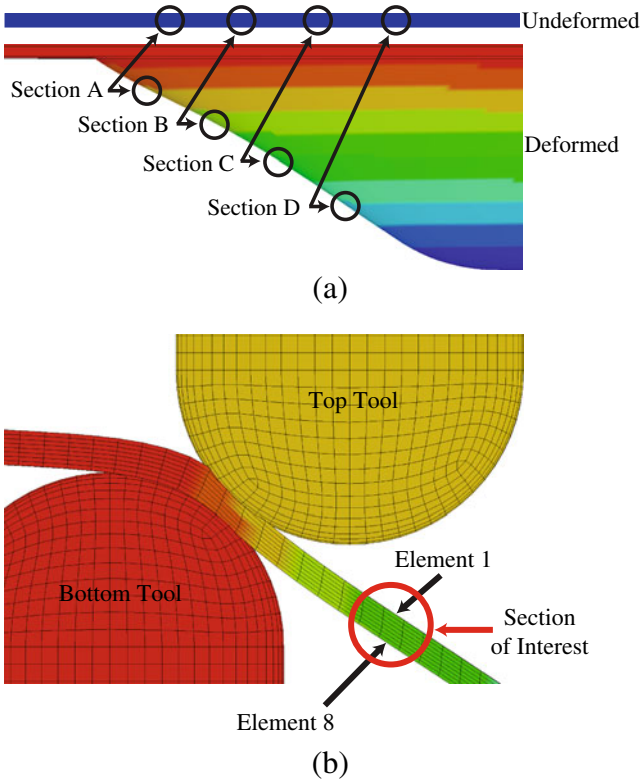

Fig. 9 Schematic showing (**a**) sections along the formed component wall at which the deformation history is examined, and (**b**) elements through the sheet thickness for which the deformation indicators are plotted for sections A-D

As mentioned in previous sections of the present work, the SPIF process elicits a great deal of springback which cause the designed and actual depths to be different. Figure 10 shows a contour of the vertical displacements of the cone contours of the SPIF and ADSIF simulations. Note that the neutral plane of the sheet is located at the top surface of the sheet prior to any deformation, and the feature edges correspond to the locations where the tool begins and ends contact with the sheet. The contours shown in Fig. 10 are from each of the simulations at the final stage of the forming process after release of the material (the tool is no longer in contact). In Fig. 10a, we can see that in SPIF, there is a considerable amount of deformation away from the edge of the feature which gives the illusion that the formed depth is over 13.5 mm. By taking into account the deformation outside the feature edges, we find that the actual feature depth is just under 11.0 mm. A comparable depth is seen in the feature created using ADSIF (Fig. 10b) after considering the amount of residual positive vertical displacement of the feature edge above the neutral plane of the sheet which yields a final depth of about 11.5 mm. We can also see in Fig. 10a that although the feature edges make an approximate 30° angle from the neutral plane of the sheet, the feature wall for the SPIF case is highly curved, making a smooth transition

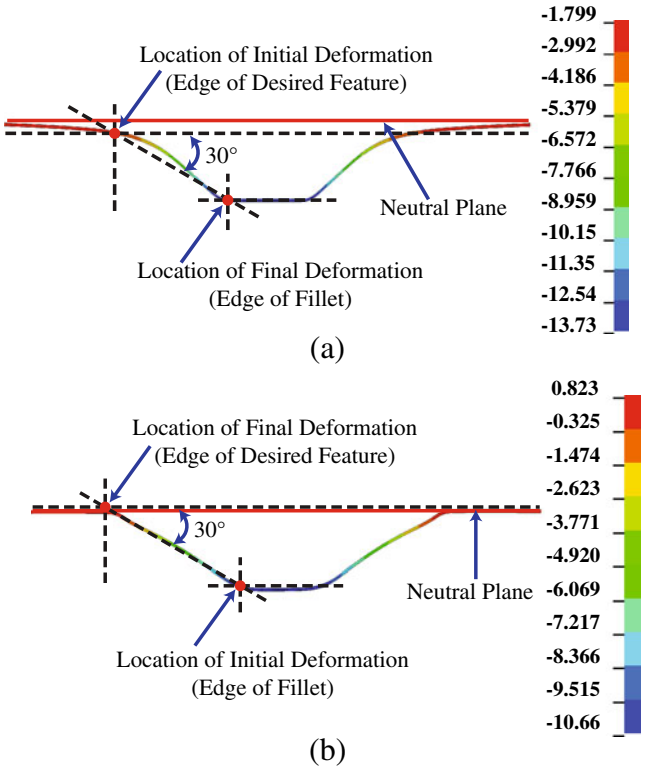

Fig. 10 Contours of the vertical positions of the cone profiles in the (**a**) SPIF and (**b**) ADSIF simulations including the location of the feature edges and the neutral plane of the sheet

from the outside the feature to the inner filets. This smooth transition shows the geometric inaccuracy of the SPIF process during the initial stages of deformation because the feature edges are not meant to have such a large radius of curvature (Fig. 5a). Figure 10b shows that the fillets at the neutral plane of the sheet are much better in the ADSIF case than in the SPIF case. The ADSIF simulation also yielded a feature wall of approximately 30° that was quite straight and thus closely matched the geometry of the intended feature (Fig. 5b).

The deformation indicators at sections A through D are plotted against *Z*-depth. It should be noted that for the remainder of this work, the plots that specify the abscissa as *Z*-depth are actually plotted against the depth at which the tool has moved the top surface of the sheet during deformation. This means that the *Z*-depth is the actual displacement of the top surface relative to the neutral plane of the sheet in either the SPIF or ADSIF simulation while loaded by the tool/s.

4.1 Plastic strain evolution

Figures 11 and 12 show the evolution of plastic strain ϵ_p in the SPIF and ADSIF simulations, respectively, for sections A through D, elements 1 and 8, at each section. In ADSIF,

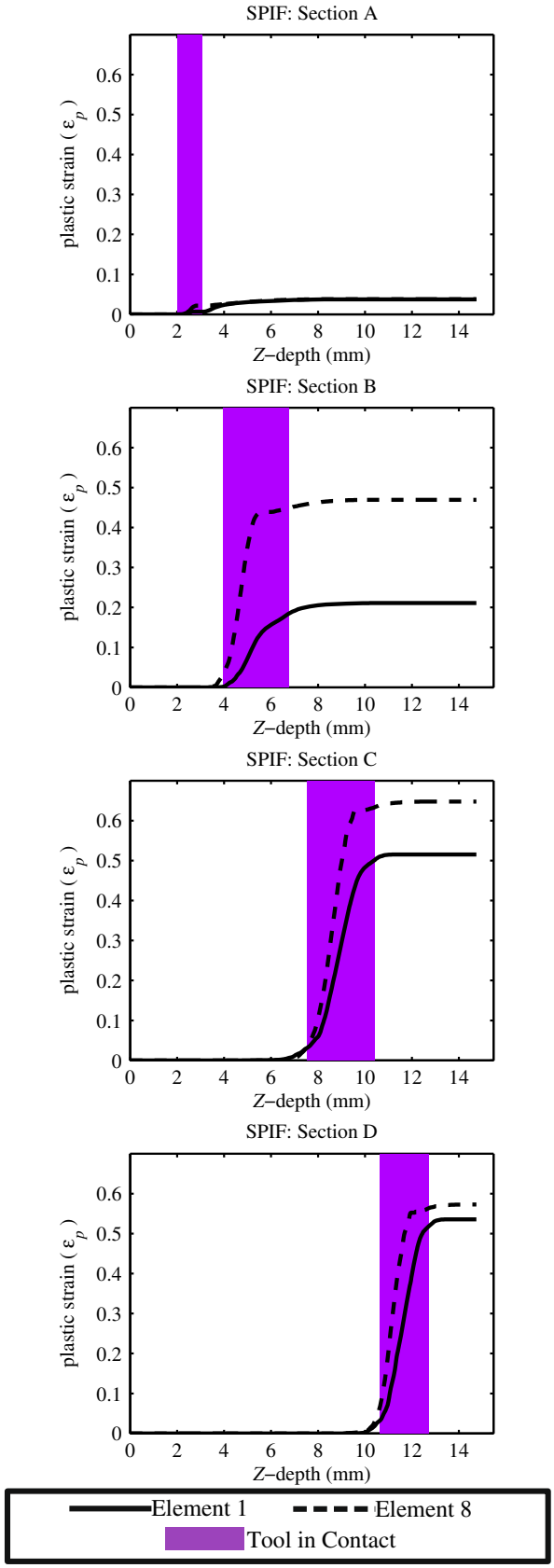

Fig. 11 Plastic strain evolution in SPIF for sections A through D, elements 1 and 8

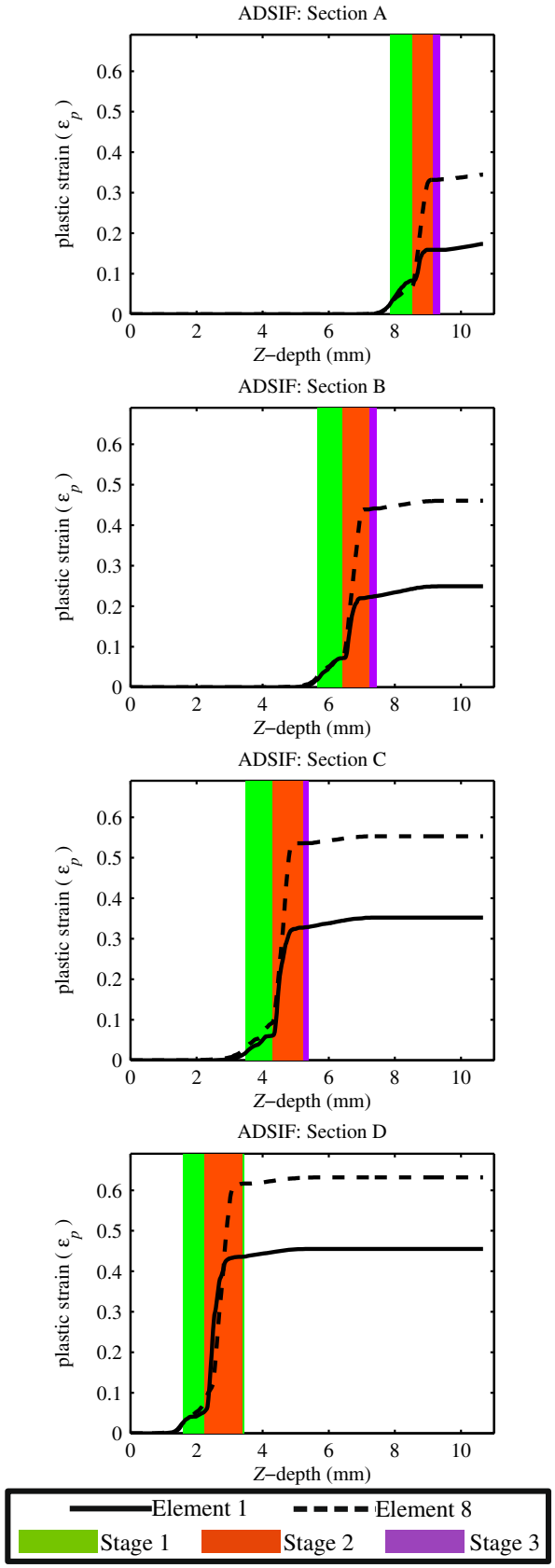

Fig. 12 Plastic strain evolution in ADSIF for sections A through D, elements 1 and 8

the deformation of a particular region of the sheet material can be decomposed into three stages of contact (Fig.13). In the first stage, a particular section of the material is in contact with one tool, i.e., the bottom tool. In this stage, the bottom tool supports and pushes the sheet in the positive *Z*-direction. In the second stage, the material is in contact with both the top and bottom tools simultaneously, which corresponds to the primary stage of deformation in the process where the sheet is being squeezed between both tools to form the sheet into the desired shape.

Subsequently, in the third stage, the material is again in contact with just one tool which is generally the top tool, but, under certain conditions, the contact could be between the sheet and the bottom tool. The plots in Fig. 12 mark these three phases during the deformation of each section distinctly for both elements 1 and 8. The evolution of plastic strain shown in Fig. 12 which corresponds to the duration of contact with the top tool only, both tools, and the bottom tool only for the ADSIF simulation are shaded in purple, orange, and green, respectively.

In SPIF, there is only one stage of contact which corresponds to the tool being in contact with a given section of the material. This stage is marked in purple in Fig. 11 as it represents contact with only the top tool. This form of denoting the contact stages during deformation of a particular section of the blank material is continued through the remainder of this paper.

Some physical trends that can be observed in Figs. 11 and 12 are as follows:

1. In ADSIF, there is a significant but consistent difference in the plastic strain between the inner (element 1) and outer (element 8) sides of the sheet of about 0.2. In SPIF, this difference ranges from 0.0 to 0.25 where the minimum is at section A, formed first in the process, followed by the maximum at section B, formed second in the process, leading to a smoothly decreasing trend until section D, the last section to be formed in the

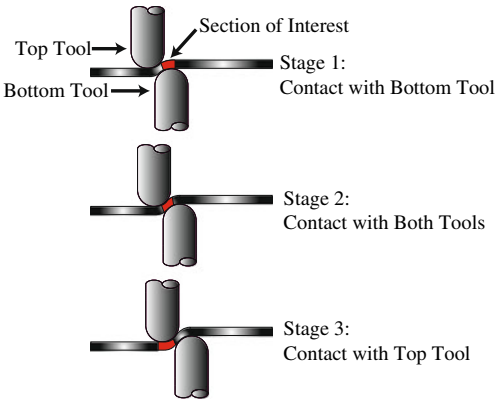

Fig. 13 Schematic showing the stages of contact for a particular section of the blank material in ADSIF

process, where the difference in effective plastic strain between the inner and outer sides of the sheet takes on a value of just under 0.05. This trend is an indicator that the primary modes of deformation change greatly in SPIF as the deformation accrues, specifically on the inner side of the sheet, whereas they are more consistent in ADSIF.

2. As shown by Malhotra et al. [7], the sheet bends locally around the forming tool in SPIF. This is the primary reason for larger plastic strain on the outer side of the sheet (element 8) which is being stretched as compared to the inner side of the sheet (element 1) which is being compressed. A similar phenomenon also occurs in ADSIF. However, an additional mechanism that comes into play in ADSIF is the effects of the bottom tool. The bottom tool drags the outer side of the sheet (element 8) along the direction of tool motion as well as causing compression of the sheet between the two tools.
3. In SPIF, the amount of plastic strain tends to increase with formed depth, while in ADSIF, the opposite is true. While the authors plan to look further into this phenomenon in the future, it is proposed that the reason for the gradual decrease in plastic strain over time in the ADSIF process is closely related to the curvature of the feature being formed at a given depth.
4. Figure 12 also shows that the plastic strain at any section in ADSIF develops much more quickly during stage 2 contact, i.e., when both tools are in contact with the section, as compared to the stages when only one tool is in contact with the section (stage 1 and stage 3 contact). This sudden rise in plastic strain during stage 2 contact can again be attributed to the extra shear, compression, and stretching caused by the supporting tool.
5. The time periods when both tools are in contact with a particular section of the sheet during ADSIF are typically smaller than the tool contact period in SPIF. This means that the plastic strain in ADSIF increases almost instantaneously during the short-term contact with both tools, whereas in SPIF, the plastic strain development is more gradual and occurs over many more passes of the tool. Furthermore, the plastic strain in ADSIF shows a slight increase before the tools actually reach the section of interest. This is probably caused by shearing of the material during the radially outward motion of the tools due to bending and bunching of the material in front of the tool which causes dragging in the direction of tool motion.

To summarize, the presence of the supporting tool in ADSIF results in additional shear and compression on the outer side of the sheet during contact with just the bottom tool and additional shear and compression of both the inner and outer elements during contact with both tools as compared to SPIF. This manifests itself in two major ways in terms of its effects on the plastic strain. First, the additional compression along with the confinement of the sheet between the tools causes the difference between plastic strains on the inner and outer sides of the sheet to be consistent as deformation evolves in ADSIF, indicating better control of the plastic strain through the process and also better uniformity in the deformation mechanics throughout the process, which is not the case in SPIF. Secondly, the rise in plastic strain in ADSIF is much higher during stage 2 contact, i.e., when both tools are in contact with the sheet, as compared to that in stage 1 and stage 3 contact. In addition, the radially outward motion of the tools in ADSIF causes bunching and shearing of the material prior to stage 2 contact, followed by slight stretching after stage 2 contact, and consequently a small increase in plastic strain is present during stage 1 and stage 3 contact.

4.2 Hydrostatic pressure evolution

Figures 14 and 15 show hydrostatic pressure evolution with respect to formed depth during the contact stages of the SPIF and ADSIF simulations, respectively.

The bending and stretching of the material around the tool is observed to reverse after the tool has passed over a particular section of the sheet in the SPIF process. This phenomenon has also been observed in a previous work [7].

In stage 1 contact in the ADSIF process, i.e., when only the bottom tool is in contact with the sheet, the hydrostatic pressure in the elements on the outer side of the sheet grows in the positive direction, implying a greater state of compression, whereas on the inner side of the sheet, the elements tend to stay in a state of nearly constant tension due to bending and stretching around the bottom tool. This is inversely similar to the trend seen in the early stages of the SPIF results, where the material bends and stretches around the top tool (Fig. 14), causing compression of the inner elements while the outer elements are stretched.

Once stage 2 contact has begun, i.e., both tools are in contact with the section being examined, there is a very apparent and almost instantaneous reversal of the state of hydrostatic pressure in elements 1 and 8. Essentially, the sheet is squeezed between the tools and also stretched around the tools such that the section which was pushed upwards in the Z-direction during stage 1 contact is now being pushed radially outward and downward by the top tool (Fig. 15). This causes the top surface of the sheet to undergo large compressive loading in each section while the bottom surface of the sheet undergoes compressive loading during the initial stages of the process, although to a much smaller amount than the top surface, and then later in the process, i.e., sections A and B, the elements on the outer side of the

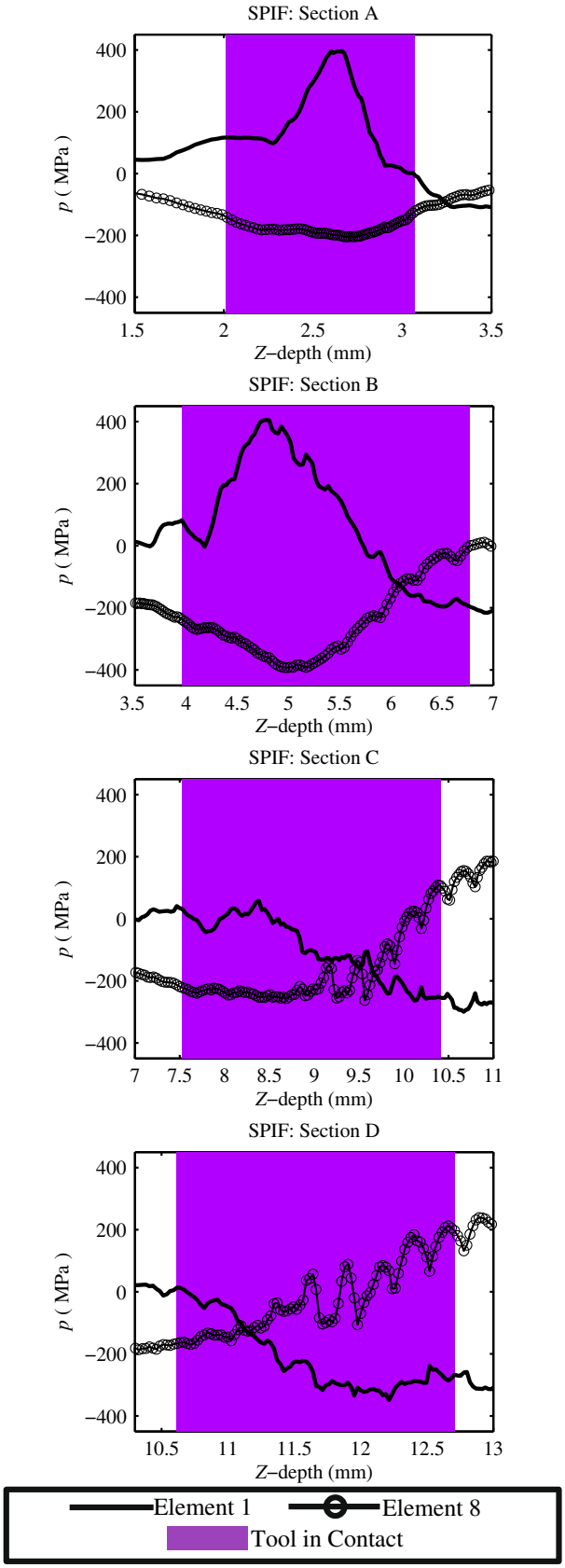

Fig. 14 Hydrostatic pressure evolution in SPIF for sections A through D, elements 1 and 8

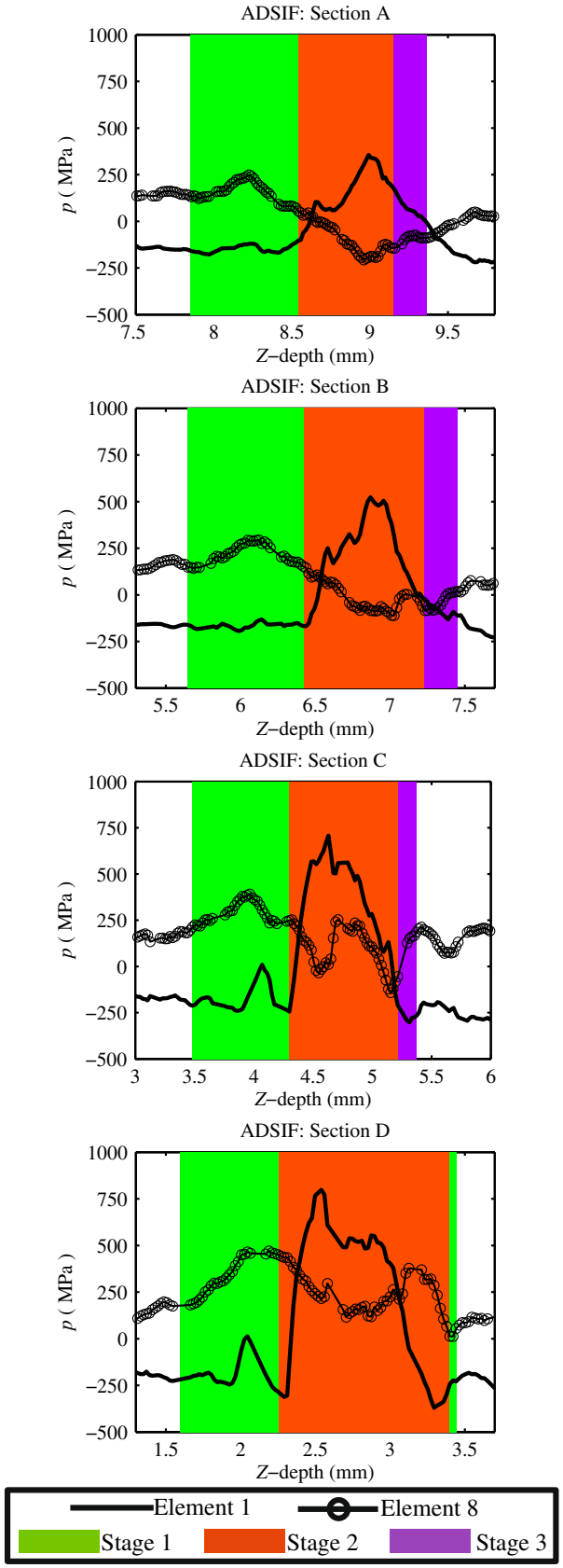

Fig. 15 Hydrostatic pressure evolution in ADSIF for sections A through D, elements 1 and 8

sheet switch to a tensile state. In the early stages of the process, the sheet is being squeezed between the tools with a minimal contribution from stretching and thus the compressive load on both the inner and outer elements. It should be noted here that the outer elements switch from a state of compression in the initial stages of the ADSIF process into a state of tension as the deformation develops. Once again, it is proposed that this also closely related to the curvature of the feature at a given formed depth, and the authors wish to further explore this theory in future work. The magnitude of the hydrostatic pressure on the outer side of the sheet (element 8) is always lower in magnitude than that on the inner side of the sheet (element 1) during stage 2 contact. This is due to the fact that the tools move in concentric circular paths of increasing radii in which the top tool, which contacts the inner surface of the sheet, must be the primary tool which pushes the sheet in the outward direction.

During stage 3 contact of the ADSIF process, the section of the blank material being examined has already been deformed and is in contact only with the top tool. The top tool during this stage of contact has a minimal effect on the overall state of hydrostatic pressure in the ADSIF process. In general, this is the start of yet another reversal process in the hydrostatic pressure such that the section is left in nearly the same state of hydrostatic pressure as that observed prior to contact with either tool.

Note that the amount of compression in ADSIF is typically much higher than in SPIF, specifically for element 1, due to the squeezing effect of the second tool which has implications in discerning an explanation for increased formability in ADSIF. Furthermore, note that the repeated bending and unbending of the material probably causes greater strain hardening than in SPIF which again has consequences on formability as well as operational performance of the formed part.

4.3 Shear strain parallel to tool motion

The magnitude of the shear strain ϵ_{ZX} parallel to the direction of motion of the tool in SPIF and ADSIF is plotted in Figs. 16 and 17, respectively. For SPIF (Fig. 16), the magnitude of the shear in element 1 is comparable to that in element 8 in the beginning of the process (sections A and B). However, as deformation accrues the magnitude of the shear strain parallel to the direction of the tool becomes much larger on the top surface of the sheet than on the bottom surface, element 1 taking on a value of nearly twice that seen in element 8 at section D. The rate of shearing of the elements in the direction parallel to tool motion is greatest during contact with the tool, staying relatively unaltered before and after contact with the tool, and the magnitude of ϵ_{ZX} increases as the depth of deformation increases until the transition from sections C to D where there was very

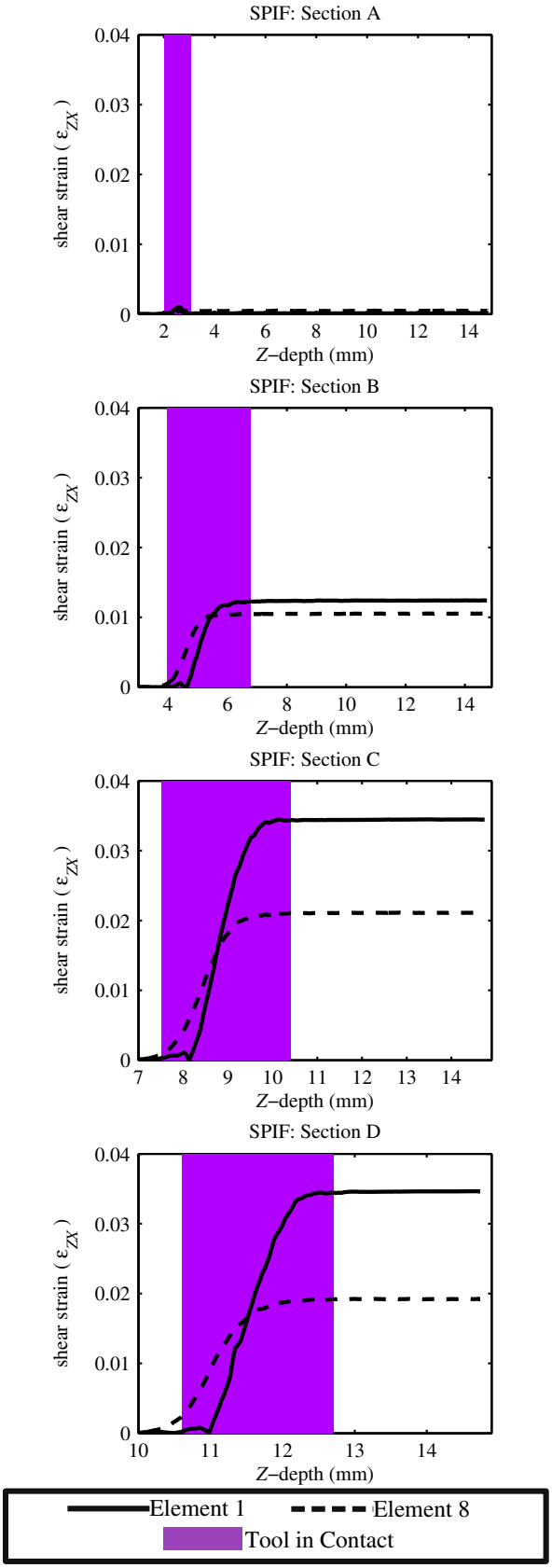

Fig. 16 Shear strain parallel to tool motion in SPIF for sections A through D, elements 1 and 8

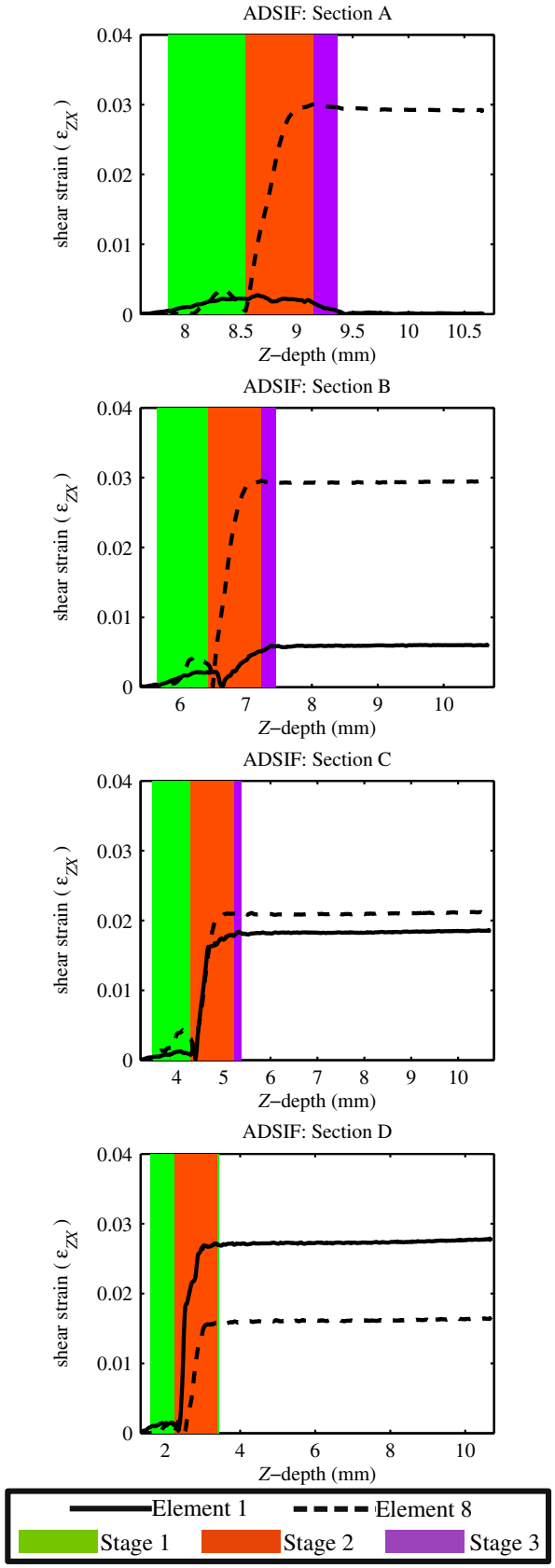

Fig. 17 Shear strain parallel to tool motion in ADSIF for sections A through D, elements 1 and 8

little change observed. These observations agree with past experimental observations by Jackson and Allwood [4] and numerical results by Malhotra et al. [7].

For ADSIF, Fig. 17 shows that ϵ_{ZX} is initially, section D, greater on the inner side of the sheet (element 1) than on the outer side of the sheet (element 8). As the deformed depth becomes greater, this trend is reversed as seen from sections A, B, and C. Also, the shear parallel to the motion of the tool in element 8 is observed to increase as the depth increases, and the opposite is true of element 1.

This is due to the fact that during the ADSIF process, the material tends to bunch up in front of the top tool, but not so much in front of the bottom tool. Therefore, the elements at the top surface of the sheet are dragged in the direction of the tool and flattened during the initial stages of deformation in ADSIF, causing greater shear in element 1. As the deformation progresses, the tendency for this material bunching reduces, and the strain trends are reversed. Note that as in the case of plastic strain evolution, the rate of deformation in ADSIF is maximized during contact with both tools, i.e., during contact stage 2. Also, the magnitude of ϵ_{ZX} is slightly greater in SPIF than in ADSIF, specifically for element 1, and the trends of ϵ_{ZX} evolution are much different between the two processes.

4.4 Shear strain perpendicular to tool motion

The evolution of shear strain in the direction perpendicular to the tool motion ϵ_{ZY} in SPIF and ADSIF is shown in Figs. 18 and 19, respectively. It can be seen that the magnitude of ϵ_{ZY} is one full order higher in ADSIF than in SPIF. This indicates that increased shear perpendicular to the motion of the tool is a significant effect of the supporting tool on the process mechanics of ADSIF. Additionally, the magnitude of ϵ_{ZY} is significantly higher than the magnitude of ϵ_{ZX} (Fig. 17) in ADSIF. The ϵ_{ZY} in ADSIF also decreases in magnitude as the depth of deformation increases (from sections D to A) and remains unchanged before and after the three stages of contact. In contrast, the magnitude of ϵ_{ZY} in SPIF is slightly less than that of ϵ_{ZX} and is quite constant before and after contact with the tool.

Figure 19 also shows a rapid increase in ϵ_{ZY} during contact with both tools in ADSIF which is similar to the phenomenon seen for the effective plastic strain and shear strain parallel to tool motion (Figs. 12 and 17, respectively). For the SPIF process, shear perpendicular to the tool travel is lesser than that parallel to it because the primary mechanism for this type of shear in SPIF is bunching of material in front of the tool via protrusion of the tool into the material. This bunching of the material is much lower in SPIF than that in ADSIF because the deformation is not as well concentrated into a local deformation region (Fig. 10). This can

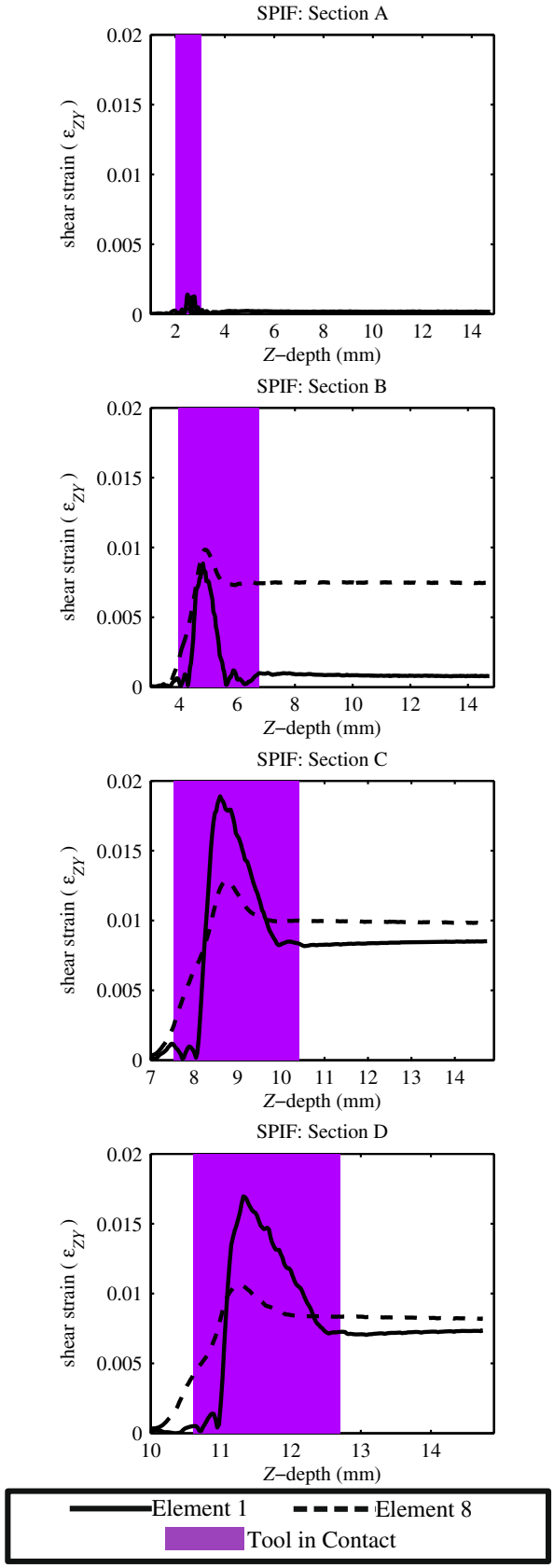

Fig. 18 Shear strain perpendicular to tool motion in SPIF for sections A through D, elements 1 and 8

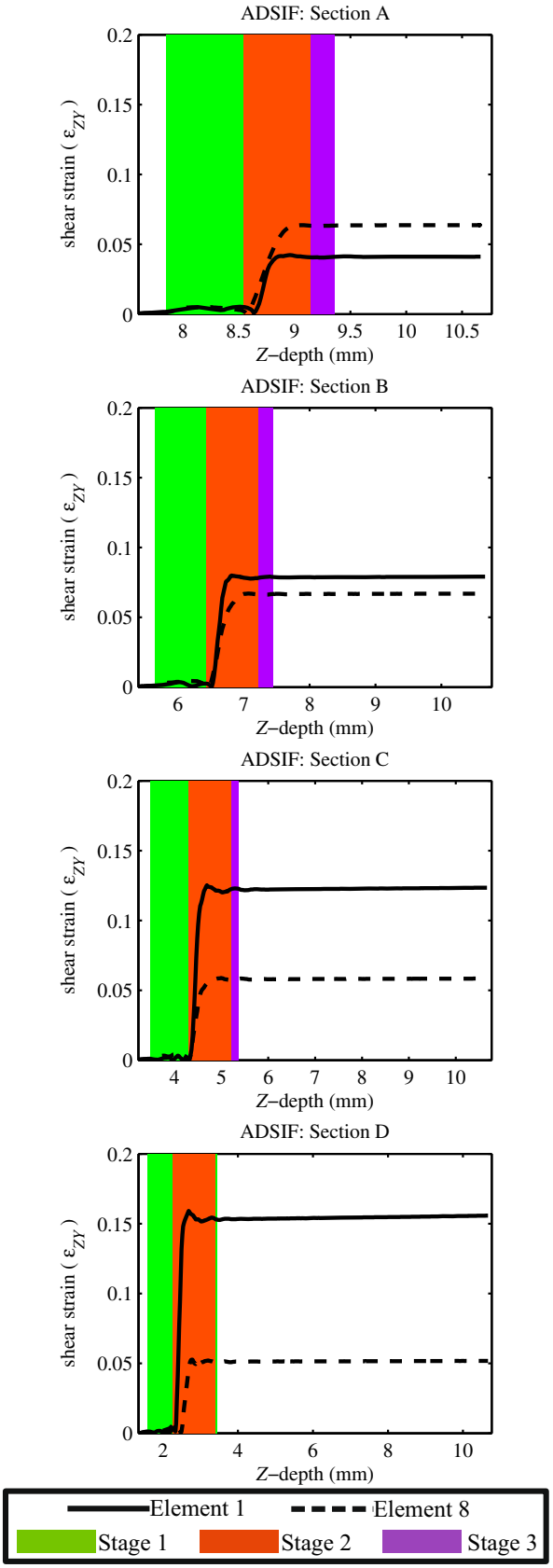

Fig. 19 Shear strain perpendicular to tool motion in ADSIF for sections A through D, elements 1 and 8

be attributed to the top tool being forced to protrude into the sheet further via the opposing force from the bottom tool in ADSIF.

5 Discussion

In this section, the authors wish to provide a discussion which focuses on the primary implications of the deformation mechanisms observed for ADSIF in the present work.

5.1 Deformation mechanisms in ADSIF

It was found in this work that the dominant modes of deformation in the ADSIF process are local bending of the sheet around the tool combined with a squeezing effect due to the outer tool as well as shear perpendicular to and parallel to the motion of the tools. It was shown that the material undergoes three different stages of contact with the tools in ADSIF which are denoted as stage 1, stage 2, and stage 3 contact (Fig. 13). It was observed that plastic strain and shear strain at a particular material section evolved fastest during stage 2 contact, i.e., when both the tools were in contact with the sheet (Figs. 12, 17, and 19). Furthermore, the magnitude of shear strain perpendicular to the motion of the tools and plastic strain in ADSIF (Figs. 12 and 19) were higher than those observed in SPIF (Figs. 11 and 18).

The sign of the hydrostatic pressure in ADSIF was found to reverse between stage 1 and stage 2 contact (Fig. 15) which indicated a bending and unbending behavior of the sheet material between these stages of contact. Additionally, it was found that the magnitude of hydrostatic pressure was much higher in ADSIF as compared with that in SPIF, especially during stage 2 contact, when both tools were in contact with the sheet simultaneously.

The higher magnitudes of shear strains and hydrostatic pressure in ADSIF as compared to SPIF indicate a significant increase in shear and volumetric deformation caused by the presence of the second tool. This is also supported by the fact that these trends were significantly magnified while both tools were simultaneously in contact with the sheet material during ADSIF.

Another difference observed between ADSIF and SPIF was the phenomenon of material bunching which manifested most prominently in terms of increased shear on the inner side of the sheet (element 1). The bunching of material ahead of the top tool along the radial and tangential directions during the initial portion of the deformation in ADSIF causes the material on the inner surface of the sheet to be first bunched up and flattened out further than those on the outer side of the sheet. This bunching phenomenon does not occur for the bottom tool as much as it does for the top tool, and therefore, the shear perpendicular to the motion of the tool is generally less on the outer side of the sheet than on the inner side of the sheet, and the magnitude of perpendicular shear on the outer side of the sheet after contact with the tools remains relatively constant over the entire deformation history, i.e., for all sections analyzed. The reason for the lack of bunching in front of the bottom tool is probably that the boundary of the material will have a tendency to create a moment and upward force to counteract the downward deformation, and thus, the protrusion of the top tool is increased, whereas the material tends away from the bottom tool. Furthermore, as the deformation proceeds, the extent of this bunching reduces. Since only one tool is used in SPIF, this material bunching phenomenon is negligible, but the shear strains are almost always higher on the inner side of the sheet in the direction parallel to the motion of the tool (Fig. 16), reaching a maximum difference in sections C and D when the shear parallel to the motion of the tool in element 1 is about twice that of element 8.

The intensity of the deformation experienced in ADSIF in the local tool contact zone as compared to SPIF was observed to be much greater.

5.2 Implications on fracture in ADSIF

The primary mechanics of deformation and fracture in SPIF have been investigated by Malhotra et al. in [7] using a damage plasticity-based finite element model. They showed that the tendency for the sheet metal to fracture during the forming process is retarded by increasing hydrostatic pressure as well by increasing through-the-thickness shear (ϵ_{ZX} and ϵ_{ZY}). This was supported by a work performed by Meier et al. [8] and by Allwood and Shouler [1]. The authors showed that the maximum strain before failure, forming forces and failure depth predicted by FEA matched quite well with those obtained from experiments [7]. It has also been shown that ADSIF is characterized by increased formability in addition to enhanced geometric accuracy and greater process flexibility [6]. The increased hydrostatic pressure and greater through-the-thickness shear in ADSIF, as shown in this work, might be the deformation mechanisms that are responsible for the increased formability observed in ADSIF, especially in light of the work mentioned previously in this section that has shown these deformation mechanisms to increase formability in sheet metal forming operations.

Note that the repeated bending–unbending nature of deformation in ADSIF causes greater material hardening than in SPIF. Furthermore, the greater hydrostatic pressure probably prevents shear bands from developing, or, once developed, the compressive load state impedes voids from growing further, thereby inhibiting complete material fracture. Both of these observations have significant and

positive implications for the operational life of components formed using ADSIF as compared to components formed using SPIF.

6 Conclusions and future work

Th ADSIF and SPIF processes are simulated in this work using FEA to study the difference in the deformation mechanics of the two processes. From a FEA point of view, it was found that artificial dynamic oscillations might occur in the SPIF simulation due to increased tool speed and due to the uncontrolled nature of deformation in SPIF. Mass damping and the use of nonreflecting boundary conditions for the sheet metal have been found to be effective in resolving these issues without causing any apparent numerical inaccuracy. For the ADSIF simulation, it was found that the constraint provided by the additional supporting tool was sufficient to circumvent these instabilities, but in order to improve the comparison, the same numerical techniques were employed for both models.

A detailed analysis of the deformation history obtained from FEA has been used to show that while ADSIF exhibits some of the traits of the SPIF process, the behavior during deformation in its entirety is much different. ADSIF is characterized by a bending–unbending nature of deformation along with squeezing of the sheet as specified in terms of three separate stages of sheet–tool contact. ADSIF also causes the sheet metal to be subjected to greater plastic strains, through-the-thickness shear strains and greater hydrostatic pressure than in SPIF. The primary cause for this is the highly localized nature of deformation in ADSIF as well as the presence of the additional supporting tool. Based on past research by the authors as well as by other authors, along with the trends in deformation mechanics observed in this work, it is proposed that the higher hydrostatic pressure and through-the-thickness shear are probably the reasons for increased formability in ADSIF.

In future work, the authors will further develop the process modeling technique for the ADSIF process to include damage and fracture of the sheet material. This information will also be used to manipulate process parameters to increase formability as well as to quantitatively predict forming forces and failure. The authors will also explore further the dependence of process mechanics on the curvature of the desired component as well as the dependence on friction at the tool–sheet interface.

Acknowledgments The authors gratefully acknowledge the support provided for this work by the National Science Foundation, USA, and the Department of Energy, USA.

References

1. Allwood JM, Shouler DR (2009) Generalised forming limit diagrams showing increased forming limits with non-planar stress states. Int J Plast 25(7):1207–1230. doi:10.1016/j.ijplas.2008.11.001
2. Emmens W, van den Boogaard A (2009) An overview of stabilizing deformation mechanisms in incremental sheet forming. J Mater Process Technol 209(8):3688–695. doi:10.1016/j.jmatprotec.2008.10.003
3. Fan J, Tang C, Tsui C, Chan L, Lee T (2006) 3D finite element simulation of deep drawing with damage development. Int J Mach Tools Manuf 46(9):1035–1044. doi:10.1016/j.ijmachtools.2005.07.044
4. Jackson K, Allwood J (2009) The mechanics of incremental sheet forming. J Mater Process Technol 209(3):1158–1174. doi:10.1016/j.jmatprotec.2008.03.025
5. Malhotra R, Cao J, Ren F, Kiridena V, Cedric Xia Z, Reddy NV (2011) Improvement of geometric accuracy in incremental forming by using a squeezing toolpath strategy with two forming tools. J Manuf Sci Eng Trans ASME 133(6):603–611. doi:10.1115/1.4005179
6. Malhotra R, Cao J, Beltran M, Xu D, Magargee J, Kiridena V, Xia ZC (2012a) Accumulative-DSIF strategy for enhancing process capabilities in incremental forming. CIRP Ann Manuf Technol 61(1):251–254. doi:10.1016/j.cirp.2012.03.093
7. Malhotra R, Xue L, Belytschko T, Cao J (2012b) Mechanics of fracture in single point incremental forming. J Mater Process Technol 212(7):1573–1590. doi:10.1016/j.jmatprotec.2012.02.021
8. Meier H, Magnus C, Smukala V (2011) Impact of superimposed pressure on dieless incremental sheet metal forming with two moving tools. CIRP Ann Manuf Technol 60(1):327–330. doi:10.1016/j.cirp.2011.03.134
9. Silva MB, Skjoedt M, Atkins AG, Bay N, Martins PAF (2008) Single-point incremental forming and formability failure diagrams. J Strain Anal Eng Des 43(1):15–35. doi:10.1243/03093247JSA340
10. Silva MB, Skjoedt M, Bay N, Martins PAF (2009) Revisiting single-point incremental forming and formability/failure diagrams by means of finite elements and experimentation. J Strain Anal Eng Des 44(4):221–234. doi:10.1243/03093247JSA522
11. Xue L (2007) Damage accumulation and fracture initiation in uncracked ductile solids subject to triaxial loading. Int J Solids Struct 44(16):5163–5181. doi:10.1016/j.ijsolstr.2006.12.026
12. Xue L (2010) Eng Fract Mech 77(8):1275–1297. doi:10.1016/j.engfracmech.2009.12.008